PSI-SR-1323

EOIL Power Scaling in a 1-5 kW Supersonic Discharge-Flow Reactor

Steven J. Davis
Seonkyung Lee
David B. Oakes
Julie Haney
John C. Magill
Dwane A. Paulsen
Paul Cataldi
Krisin L. Galbally-Kinney
Danthu Vu, Jan Polex

Presented at SPIE Photonics West LASE 2008 (San Jose, CA),
(19-24 January 2008).

EOIL power scaling in a 1-5 kW supersonic discharge-flow reactor

Steven J. Davis*, Seonkyung Lee, David B. Oakes, Julie Haney, John C. Magill,
Dwane A. Paulsen, Paul Cataldi, Kristin L. Galbally-Kinney, Danthu Vu, Jan Polex,
William J. Kessler, and Wilson T. Rawlins
Physical Sciences Inc., 20 New England Business Center, Andover, MA, USA 01810-1077

ABSTRACT

Scaling of EOIL systems to higher powers requires extension of electric discharge powers into the kW range and beyond with high efficiency and singlet oxygen yield. We have previously demonstrated a high-power microwave discharge approach capable of generating singlet oxygen yields of ~25% at ~50 torr pressure and 1 kW power. This paper describes the implementation of this method in a supersonic flow reactor designed for systematic investigations of the scaling of gain and lasing with power and flow conditions. The 2450 MHz microwave discharge, 1 to 5 kW, is confined near the flow axis by a swirl flow. The discharge effluent, containing active species including $O_2(a^1\Delta_g, b^1\Sigma_g^+)$, $O(^3P)$, and O_3, passes through a 2-D flow duct equipped with a supersonic nozzle and cavity. I_2 is injected upstream of the supersonic nozzle. The apparatus is water-cooled, and is modular to permit a variety of inlet, nozzle, and optical configurations. A comprehensive suite of optical emission and absorption diagnostics is used to monitor the absolute concentrations of $O_2(a)$, $O_2(b)$, $O(^3P)$, O_3, I_2, $I(^2P_{3/2})$, $I(^2P_{1/2})$, small-signal gain, and temperature in both the subsonic and supersonic flow streams. We discuss initial measurements of singlet oxygen and I* excitation kinetics at 1 kW power.

Keywords: Electric oxygen iodine laser, microwave discharge, kinetics

1. INTRODUCTION

The Electric Oxygen-Iodine Laser, EOIL, uses electric-discharge-generated $O_2(a^1\Delta_g)$ and $O(^3P)$ to produce lasing action on the $I(^2P_{1/2}\rightarrow{}^2P_{3/2})$ line at 1315 nm.[1-4] Atomic oxygen rapidly dissociates the fuel I_2, and the metastable $O_2(a^1\Delta_g)$ excites the $I(^2P_{1/2})$ state via near-resonant energy transfer:

$$O_2(a^1\Delta_g) + I(^2P_{3/2}) \rightleftarrows O_2(X^3\Sigma_g^-) + I(^2P_{1/2}) \quad (1)$$

Reaction (1) favors $I(^2P_{1/2})$ formation at lower temperatures, so the power extraction is usually done in a supersonic flow. Atomic oxygen also quenches $I(^2P_{1/2})$,

$$O + I(^2P_{1/2}) \rightarrow O + I(^2P_{3/2}) \quad (2)$$

and so its concentration must be carefully controlled to optimize the performance. This can be accomplished through addition of either NO_2 or NO to the flow:[1-3]

$$O + NO + M \rightarrow NO_2 + M \quad (3)$$

$$O + NO_2 \rightarrow NO + O_2 \quad (4)$$

A more complete set of the most relevant elementary reactions is listed in Table 1.

*sdavis@psicorp.com; phone 1 978 689 0003; fax 1 978 689 3232; psicorp.com

Table 1. Principal elementary reactions for the reaction of active-O_2 with I_2 in the MIDJet/EOIL reactor

Primary	*Secondary*
$O + O_2 + M \rightarrow O_3 + M$	$I^* + O_2(a) \rightarrow I + O_2(b)$
$O + O_3 \rightarrow O_2 + O_2$	$I^* + O_2(a) \rightarrow I + O_2(a)$
$O + I_2 \rightarrow I + IO$	$O_2(b) + O \rightarrow O_2(a) + O$
$O + IO \rightarrow I + O_2$	$O_2(b) + O \rightarrow O_2 + O$
$O_2(a) + I \rightarrow O_2 + I^*$	$O_2(b) + wall \rightarrow O_2(a)$
$O_2 + I^* \rightarrow O_2(a) + I$	$O_2(b) + I_2 \rightarrow O_2 + I + I$
$O + I^* \rightarrow O + I$	$O_2(b) + I_2 \rightarrow O_2(a) + I_2$
$O_3 + I^* \rightarrow IO + O_2$	$O_2(b) + I_2 \rightarrow O_2 + I_2$
$I + O_3 \rightarrow IO + O_2$	$O_2(a) + I_2 \rightarrow O_2 + I_2^*$
$O + NO + M \rightarrow NO_2 + M$	$O_2(a) + I_2 \rightarrow O_2 + I_2$
$O + NO_2 \rightarrow NO + O_2$	$O_2(a) + I_2^* \rightarrow O_2 + I + I$
$O_3 + NO \rightarrow NO_2 + O_2$	$I_2^* + O_2 \rightarrow I_2 + O_2$
$I^* + NO \rightarrow I + NO$	$I_2^* + He \rightarrow I_2 + He$
$I^* + I_2 \rightarrow I + I_2$	$I^* + I \rightarrow I + I$
	$IO + IO \rightarrow O_2 + I + I$
	$IO + NO \rightarrow I + NO_2$

Successful scale-up of the EOIL concept to higher powers requires several key steps:

(1) Optimization of the discharge to produce the highest possible yields of $O_2(a)$ at low ratios of power to flow rate,
(2) Manipulation of the subsonic discharge effluent chemistry to minimize the interfering effects of O and other active-oxygen species in the flow,
(3) Implementation of schemes for injecting and mixing the reagent gas I_2 to promote complete dissociation while also minimizing I* loss via O + I* quenching, to enhance the optical gain, and
(4) Design of the supersonic flow/resonator section to address boundary layer growth, optimize the $O_2(a)$ power above the gain threshold, and optimize the power extraction dynamics.

In addition, there remain significant chemical kinetics questions regarding the chemistry of O, $O_2(a^1\Delta_g)$, O_3, and NOx in the discharge effluent flow, and the reactions of these species with I_2, $I(^2P_{3/2})$, and $I(^2P_{1/2})$. In particular, our previous kinetics investigations in a small scale, subsonic reactor have shown that there is an additional, unidentified, I* loss mechanism besides Reaction (2) which limits the gain that can be achieved.[5] We describe here a microwave-driven, supersonic discharge-flow reactor designed to address these scaling and kinetics issues.

We previously reported a microwave-discharge-driven singlet oxygen generator, MIDJet, capable of producing $O_2(a)$ yields of 20-30% in dilute O_2/He mixtures at pressures of ~50 torr and discharge power of 1 kW.[6] This device is based on commercially available high-power microwave technology, and operates at powers of 1 to 5 kW; similar magnetron supplies are commercially available for powers up to ~100 kW. Based on the $O_2(a)$ yield measurements for a power/flow rate ratio of 25 kJ/mole, we noted that increasing the flow rate to achieve <10 kJ/mole could result in power efficiencies >25% for total singlet oxygen production. In addition, the observed $O_2(a)$ yields are far above the gain thresholds typical of supersonic flow (e.g. 4% at 150 K), and are appropriate for investigations of gain and power extraction at mid-scale discharge powers. We have now implemented the MIDJet discharge system in a bench-scale supersonic flow reactor with extensive optical access, for a combination of scaling and kinetics studies at 1 to 5 kW discharge power. This paper describes the reactor design, performance characterization, and initial observations of gain and lasing at 1 kW discharge power.

2. MIDJET EOIL APPARATUS

A diagram of the apparatus configured for gain measurements is shown in Figure 1. The reactor is designed to provide 2-D supersonic flow with an optical path length of 5 cm across the flow, and incorporates chilled-water cooling of the discharge effluent flow to achieve subsonic plenum temperatures near room temperature. The reactor is made of aluminum and is internally coated with Teflon to mitigate $O_2(a)$ wall loss. The MIDJet discharge chamber operates at 2450 MHz; the microwave power is injected coaxially into a tuned cavity. The discharge feedstock gas, typically a dilute mixture of O_2 in He, enters the MIDJet discharge chamber through a series of circumferentially mounted tangential inlets, resulting in a swirl flow that confines the active discharge to a coaxial volume in the center of the chamber. The discharge effluent expands into a short section of 1-inch (i.d.) axisymmetric flow, and then through a water-cooled transition section which transforms the flow into a rectangular duct 1 cm high and 5 cm across. The 2-D subsonic flow then passes through a multiport optical cell, which is equipped with three pairs of circular windows along the side for optical emission and absorption probes and a large rectangular window on the top for spanwise imaging. Downstream of the cell and immediately (~1 ms flow time) upstream of the supersonic nozzle, I_2 with a He carrier is injected from the top and bottom of the duct through a series of sonic orifices distributed across the span. The reacting flow then passes through a contoured supersonic nozzle (1.5 mm throat height) designed by the method of characteristics to produce Mach 2.6 flow at the nozzle exit. Beyond the nozzle exit, the flow channel diverges with a half-angle of 4 degrees to offset boundary layer growth. Initial experiments also used a 2-degree half-angle as described below. The supersonic flow channel has full-length optical windows mounted on each side for optical access by emission, gain, and imaging diagnostics. The reactor length is 60 cm from the discharge exit to the nozzle throat, and 12 cm from the nozzle throat to the end of the divergent supersonic flow section. The reactor is pumped through a high-conductance gate valve and foreline by a 2150 cfm(air) blower/forepump combination.

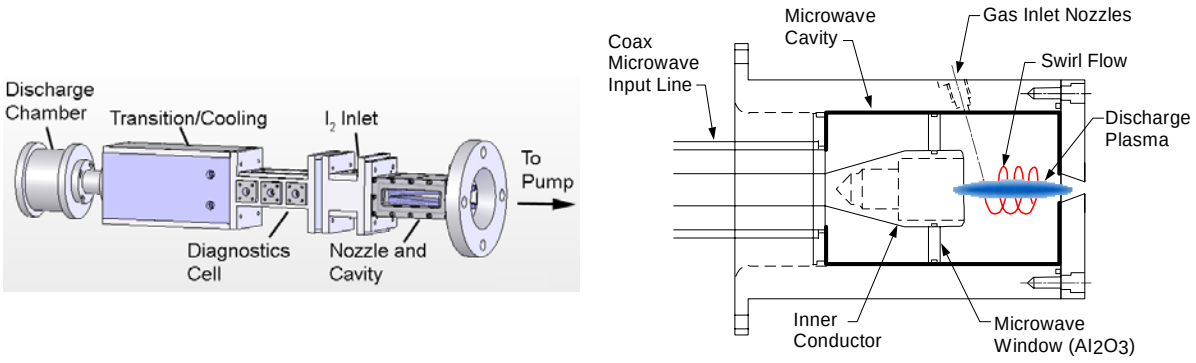

Figure 1. MIDJet EOIL reactor. (a) Supersonic microwave discharge flow reactor; (b) Discharge chamber.

Typical flow and pressure conditions for 1 kW operation are 40-80 mmole/s, 30-70 torr in the discharge chamber, 22-45 torr in the subsonic flow duct, and 0.7-1.4 torr in the supersonic flow exit. The corresponding E/N of the discharge is 15-40 Td at 1 kW. The flow velocities are ~8500 cm/s in the subsonic section and Mach ~2 in the supersonic section (see below). Typical flow temperatures are ~500 K immediately downstream of the discharge exit, 300-350 K in the 2-D subsonic plenum flow, and 130-150 K in the supersonic flow. These temperatures are determined by a combination of thermocouple measurements, $O_2(a \rightarrow X)$ rotational temperatures, and $I \rightarrow I^*$ absorption/gain line widths (see below). Flows of I_2 are generated by passing a helium carrier flow over a bed of iodine crystals at temperatures ranging from room temperature to 55 C, resulting in I_2 flow rates from 2 to 30 μmole/s. I_2 concentrations and flow rates are determined by absorption measurements at 488 nm using a spectrally filtered LED absorption photometer at the outlet of the heated iodine cell. The entire reactor has a modular design for ease of changing reagent inlet, cooling, nozzle, and diagnostic configurations; additional lengths of water-cooled subsonic ducts and reagent inlet modules are available but are not shown in Figure 1.

The primary optical diagnostics are absolute spectral emission measurements of $O_2(a \rightarrow X)$ at 1270 nm and $I^* \rightarrow I$ at 1315 nm, and gain/absorption measurements on the F"=4 – F'=3 hyperfine line of the I – I* transition at 1315 nm. The emission diagnostic is a fiber-coupled, near-infrared InGaAs array monochromator which is calibrated for absolute

responsivity; analysis of the spectra gives concentrations of $O_2(a)$ and I*, as well as $O_2(a)$ rotational temperatures.[4-7] The gain diagnostic is a scanning tunable diode laser transmission spectrometer; rapid scanning of the laser wavelength across the atomic line gives a direct measure of the absorption or gain of the medium.[5,7] In addition, analysis of the width of the line gives the temperature of the gas, and the magnitude of the absorption or gain signal gives the quantity ([I*]-[I]/2). Combination with the [I*] measurements by emission gives determinations of [I], the inversion ratio [I*]/[I], and the dissociation fraction of the injected I_2. Additional diagnostics include a fiber-coupled 580 nm air-afterglow photometer for detection of O-atoms (via the O + NO chemiluminescence), and high-sensitivity absorption photometers for O_3 (254 nm) and I_2 (488 nm). These methods are all described elsewhere.[5,7]

3. PERFORMANCE CHARACTERIZATION: FLOWFIELD AND YIELDS

We computed the properties of the supersonic flowfield using the FLUENT® CFD code. The calculations used the experimentally observed plenum pressure and temperature conditions, laminar flow, and no slip at the walls. Computed Mach number fields are shown in Figure 2 for 2 degree and 4 degree expansion ramps. The 2 degree ramp shows substantial boundary layer growth limiting the Mach number to <2. The corresponding flow temperatures are 200 to 250 K. The computed temperatures and densities were confirmed by NIR emission measurements of $O_2(a)$ rotational temperatures and number densities. The calculations for the 4 degree ramp show significantly less boundary layer effect and higher Mach numbers. The computed on-axis temperatures and number densities are compared to experimental observations in Figure 3. The $O_2(a)$ emission diagnostic averages over the full vertical extent of the flow, including the boundary layer, and thus determines apparent rotational temperatures of ~180 K, slightly higher than the computed on-axis temperatures near 150 K. The I-atom measurements sample a small volume on the flow axis, and give temperatures in good agreement with the calculated values. To compare the measured and computed number density profiles, we normalized the computed profile to the observed subsonic $O_2(a)$ number density (with no added I_2). The measured supersonic $O_2(a)$ number densities are in very good agreement with the computed profile.

Typical $O_2(a)$ yields for 50 mmole/s are shown in Figure 4. These yields were determined by $O_2(a \rightarrow X)$ emission measurements in the subsonic diagnostic cell. Additional measurements at a window just downstream of the discharge exit give essentially the same yield for a given O_2 mole fraction, signifying no net loss of $O_2(a)$ along the subsonic flow section. The yield increases with decreasing O_2 mole fraction, as we expect due to the corresponding increase in characteristic electron energy of the discharge.[5,6,8] We have focused our gain measurements on the 5% O_2 case, for which the $O_2(a)$ yield is ~20%.

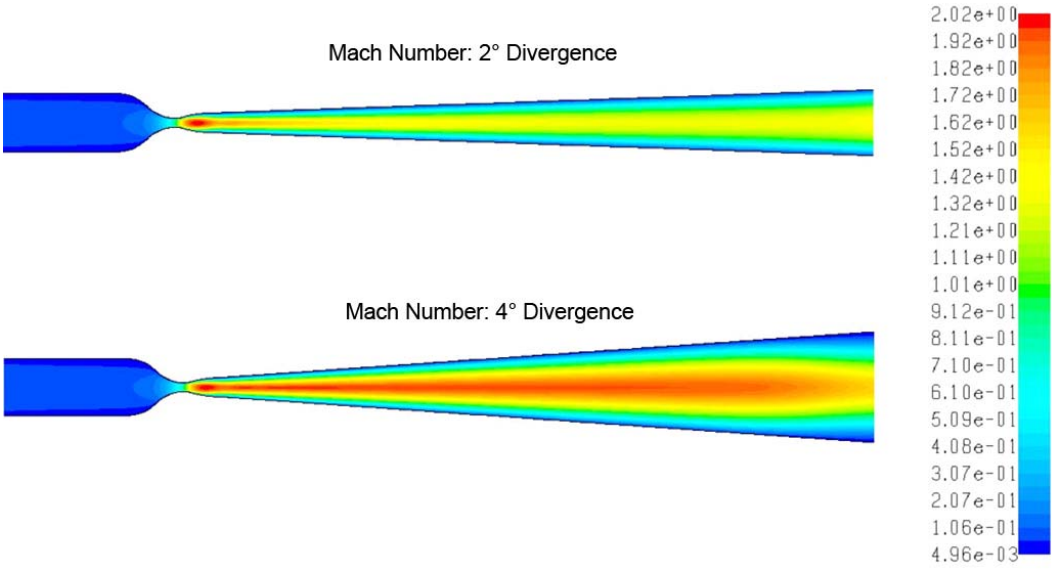

Figure 2. CFD calculations of Mach number distributions in 2-D supersonic flow field.

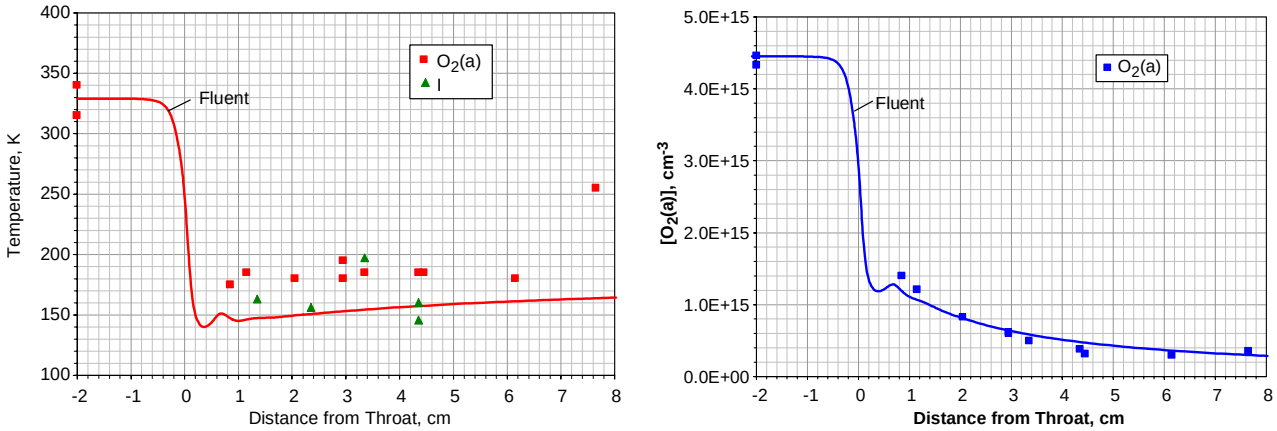

Figure 3. Comparison of flow diagnostic measurements and CFD calculations, for 4 deg divergence, 5% O_2/He. (a) Temperature; (b) Number density.

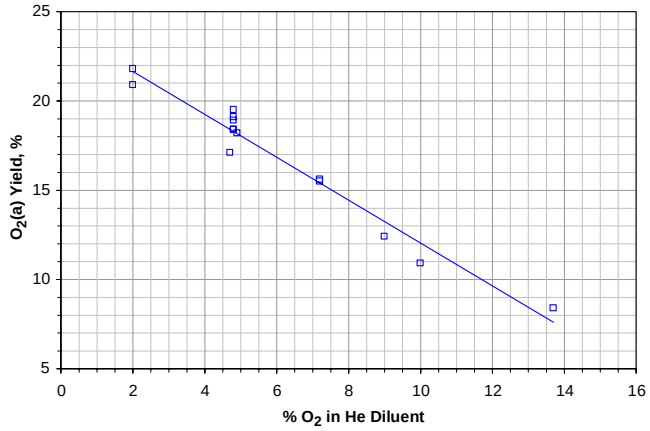

Figure 4. MIDJet/EOIL $O_2(a)$ yields: 1 kW discharge power, 50 mmole/s, 25-45 torr.

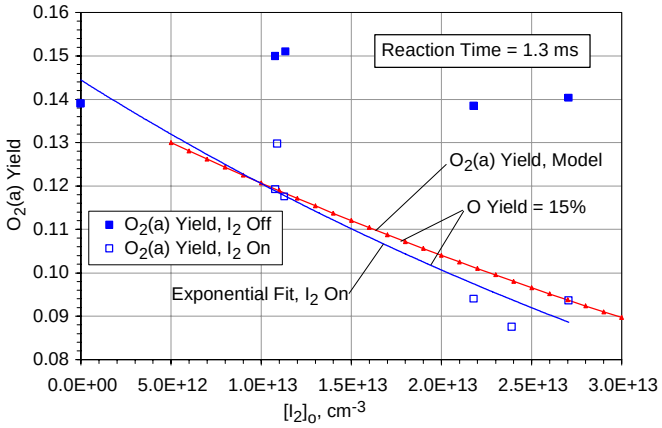

Figure 5. $O_2(a)$ loss in subsonic flow section due to I* quenching by O.

Atomic oxygen yields were estimated from the loss of $O_2(a)$ incurred upon injection of I_2 into the subsonic flow. For the condition $[O] >> [I_2]_o$, I_2 dissociation is prompt, and Reactions (1) and (2) enter into a quasi-steady state, where quenching conversion of I* to I results in a concomitant loss of $O_2(a)$:

$$-d\{\ln[O_2(a)]\}/dt = k_1k_2[I][O] / \{k_{-1}[O_2] + k_2[O]\} \quad (5)$$

We have previously used this relationship to determine the rate coefficient k_2 from measurements of the first-order $O_2(a)$ loss rate for known [O], [I], and $[O_2]$.[5] For the present case, we observe strong I→I* absorption, signifying $[I^*] << [I] \sim 2[I_2]_o$, and we can estimate [O] from the observed first-order $O_2(a)$ loss rate for a given $[I_2]_o$. An example data set is shown in Figure 5, where I_2 was injected upstream of the subsonic optical cell and the $O_2(a \rightarrow X)$ emission intensity was observed as a function of $[I_2]_o$ for a reaction time of 1.3 ms. For each condition, the $O_2(a)$ yield was determined with the I_2 flow on and off. The solid curve is an exponential fit to the $O_2(a)$ loss data, and gives a slope, $-d\{\ln[O_2(a)]\}/d[I_2]_o$, corresponding to an O yield of 15%, compared to an initial $O_2(a)$ yield of 14-15% for this discharge condition. The other curve in the figure is from an analytical model using the above steady-state relationship for an assumed O yield of 15%, and gives good agreement with the data and the first-order loss rate approximation. As an alternative approach, where I_2 is injected immediately upstream of the nozzle throat, we observe $O_2(a \rightarrow X)$ emission in the supersonic flow with the I_2 flow on and off. In this case, the reaction time is primarily the subsonic flow time between the injector and the nozzle throat, ~1 ms, and the ratio of the two emission signals can be used to estimate the first-order $O_2(a)$ loss rate in the subsonic flow. This is illustrated by the supersonic $O_2(a \rightarrow X)$ spectra shown in Figure 6. These measurements typically give O yields comparable to the yields of $O_2(a)$, i.e. ~20% for the 5% O_2/He mixture at 50 mmole/s and 1 kW. For low I_2 flow rates, the O + I* quenching

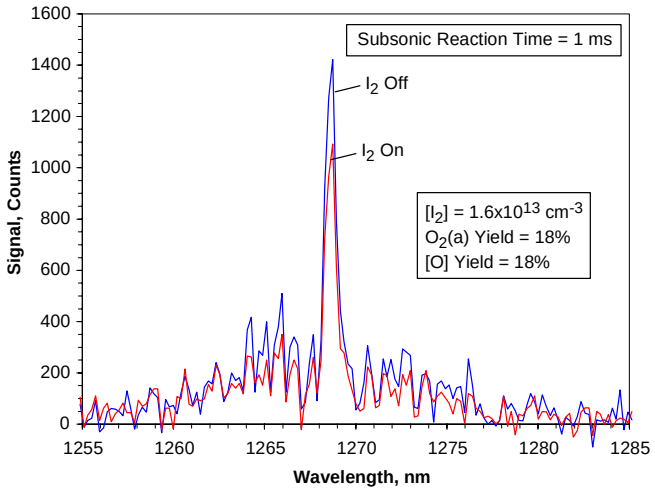

Figure 6. $O_2(a)$ loss observed in supersonic flow, due to O + I* in the subsonic reaction zone.

process results in only a 20-30% loss in $O_2(a)$ yield delivered to the supersonic cavity. However, as indicated in Equation (5), the loss of $O_2(a)$ related to O + I* quenching increases with I_2 concentration, and can severely deplete the $O_2(a)$ yield if not arrested by the addition of NOx (Reactions (3) and (4)). This is an extremely important consideration for scaling to higher gain, which requires injection of higher $[I_2]_o$.

4. OBSERVATIONS OF GAIN AND LASING

Example results of our first gain measurements at 1 kW discharge power are shown in Figure 7. The experimental conditions for these measurements were: 5% O_2/He at 47 mmole/s with ~0.4 mmole/s NO added through the discharge, 33 torr in the MIDJet discharge, 24 torr in the 2-D subsonic flow. The supersonic flow was probed by the diode laser 4.35 cm downstream of the nozzle throat. The diode laser transmission scans are shown for NO off (absorption) and on (gain), for an iodine source temperature of 37 C (~5 μmole/s, $[I_2]_o \sim 7 \times 10^{13}$ cm^{-3} in the subsonic flow). The scans have been corrected for etalon baselines, and are fit to Gaussian curves representing Doppler broadening. The line widths correspond to temperatures of ~135 K. Measurements further upstream, ~2 cm downstream of the throat, showed slightly smaller positive gain. We also performed experiments with up to 16% O_2 in He, which showed smaller but still positive gain. In very recent work, we have increased the iodine source temperature to attain I_2 flow rates up to 33 μmole/s and peak gains up to 0.025 %/cm, for a total flow rate of 82 mmole/s and 70 torr in the discharge.

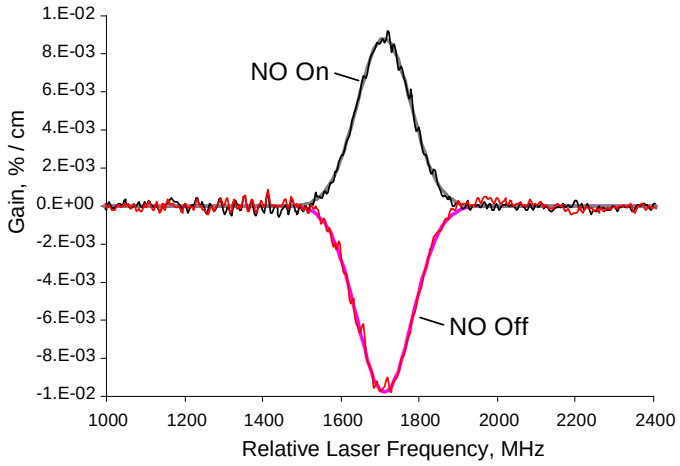

Figure 7. MIDJet/EOIL gain measurement at low I_2 flow rate: 4.35 cm downstream of nozzle throat, 5% O_2/He at 47 mmole/s + 0.4 mmole/s NO + 5 μmole/s I_2, 1 kW discharge power.

In all of our experiments, addition of NO is a key requirement for producing optical gain. From the steady-state relationship in Equation (5), without NO, we expect to observe small, positive gains (few x 10^{-3} %/cm) for $[I_2]_o$ less than about 1 x 10^{14} cm^{-3}, and increasing absorption above that level. In contrast, we consistently observe absorption at low $[I_2]_o$, even though the $O_2(a)$ yield delivered to the supersonic flow is well above the equilibrium threshold for inversion. In the examples illustrated above, direct measurements of the $O_2(a \rightarrow X)$ emission in the supersonic flow show that the $O_2(a)$ yield in the supersonic flow is ~15%, depleted from 20% by O + I* quenching in the subsonic reaction zone. At the nominal supersonic flow temperature of 150 K, the equilibrium threshold yield for inversion is ~4%. However, we observe absorption (negative gain) of ~0.01 %/cm. Clearly, there exists an additional, large, I* loss term, however this loss does not appear to cause a concomitant loss of $O_2(a)$. We have previously noted a similar effect in low-pressure subsonic flow.[5,7] The addition of NO through the discharge reduces the O + I* quenching effect, as well as the efficacy of the unknown I* loss process, resulting in positive gain.

The NO flow rate must be carefully optimized to produce maximum gain for a given I_2 flow rate. Addition of too much NO causes too much O removal via reactions (3) and (4), such that O is not in sufficient excess over I_2 to give adequate I_2 dissociation. In addition, the optimum NO flow rate decreases with increasing I_2 flow rate: at higher $[I_2]_o$, the O concentration at the I_2 inlet must be higher, and the O + I* quenching loss is more severe because of both the higher [O] and the increasing $O_2(a)$ loss with increasing [I] reflected in Equation (5). Example measurements of the NO dependence at low I_2 flow rate are shown in Figures 8 and 9. In Figure 8, the gain is optimized at 0.4 to 0.5 mmole/s of NO, and decreases at higher NO flow rates. The $O_2(a)$ yield in the subsonic flow is clearly enhanced by addition of NO through the discharge, as noted elsewhere,[9,10] however the effect is small for our conditions of high flow velocity and short reaction time. The O yield, observed by air-afterglow emission in the subsonic flow upstream of the reaction zone, is reduced exponentially at rates consistent with Reactions (3) and (4). The supersonic behavior of I and I*, extracted from gain and I* emission measurements 4.3 cm downstream of the throat, are shown in Figure 9. The total-I balance, ([I*] + [I])/2, is consistent with 100% dissociation of the injected $[I_2]_o$, for NO flow rates below 0.5 mmole/s. Above that value, the dissociation fraction clearly decreases, indicating over-titration of the O. However, the inversion ratio [I*]/[I] continues to increase, as I* loss is further reduced by increasing NO. These observations suggest that an alternative means of I_2 dissociation, such as pre-dissociation by a secondary discharge, could significantly augment the gain.

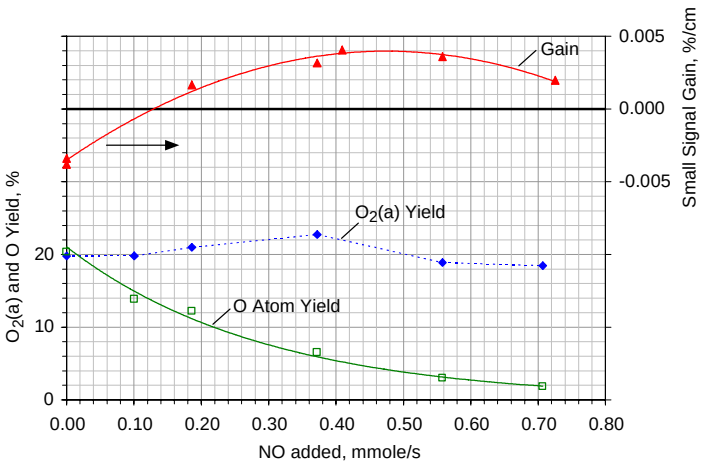

Figure 8. Effect of NO on gain and yields: 4.35 cm downstream of nozzle throat, 5% O_2/He at 47 mmole/s, 4.6 μmole/s I_2, 1 kW discharge power.

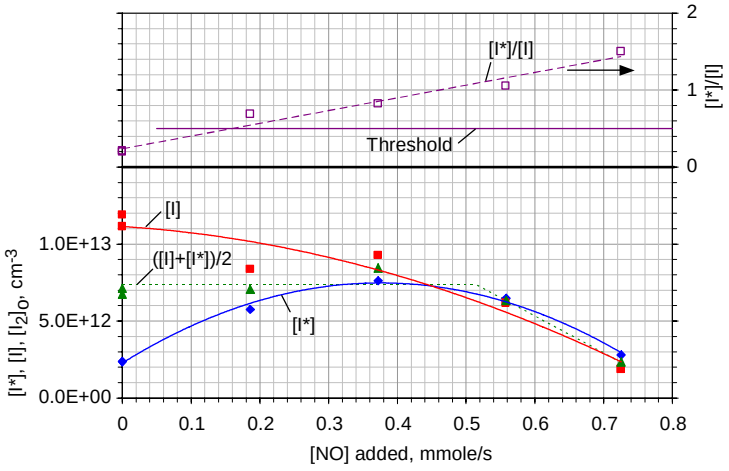

Figure 9. Effect of NO on [I] and [I*], conditions given in Figure 8.

For the initial lasing experiments, we built a resonator which can be mounted on the sides of the supersonic flow cell in place of the windows. The assembly includes He purge ports to prevent contamination of the mirrors. We used two 1-inch diameter mirrors with reflectivities of 99.997%, generously provided by Dr. David Carroll of CU Aerospace. Each mirror was mounted on a three-point tilt control and was set back some 6.5 inches from the side edge of the 2-D supersonic flow field, on opposite sides of the flow. The spanwise flow dimension (gain length) was 5 cm across. The output power was observed with power meters on both the front and back sides of the cell. The flow conditions were the same as those described above, viz. 5% O_2 in He at 47 mmole/s with ~0.4 mmole/s NO through the discharge, 33 torr in the MIDJet discharge, 24 torr in the 2-D subsonic flow, 1 kW discharge power. The I_2 generator was heated to various controlled temperatures ranging from 35 to 45 C. The mirrors were centered ~4.35 cm downstream of the nozzle throat. Laser output up to 20 mW was readily observed upon proper alignment of the mirrors. An image of the laser beam is shown in Figure 10. In very recent work at higher gain and with an improved purge flow design on the resonator, we have observed power extraction up to 110 mW, for a total flow rate of 82 mmole/s and 70 torr in the discharge.

Figure 10. Image of 1315 nm laser spot.

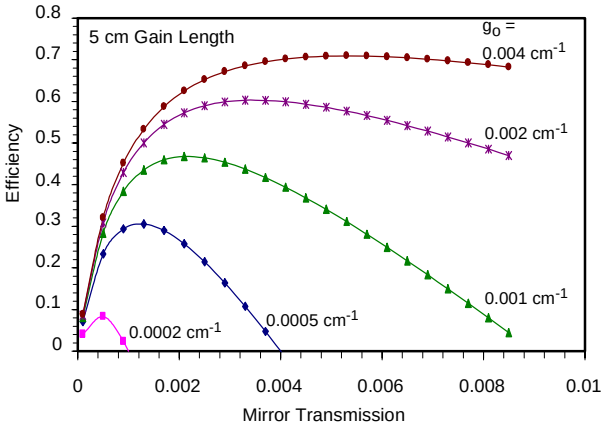

Figure 11. Scaling of resonator power extraction efficiency for 5 cm gain length.

From the observed $O_2(a)$ yield for the 47 mmole/s case, the total singlet oxygen power in the flow was 41 W, and the corresponding power above threshold was 33 W at 150 K. The power extraction efficiency was thus very low, as we expected from the Rigrod relationship for high mirror reflectivity and low gain. Calculations of the resonator extraction efficiency for a 5 cm gain length are shown in Figure 11. For low gain and high mirror reflectivity, the power extraction efficiency is very small, however for gains above about 0.2 %/cm, the extraction efficiency becomes quite large and is much less dependent on mirror transmission. In addition, for low gain, the stimulated emission rate is slow with respect to the flow velocity through the 1-inch field of view (1.4×10^5 cm/s, residence time ~20 μs). As the gain is increased, e.g. by increasing the added I_2 concentration and/or tailoring the kinetics of the system, both the optical efficiency and the radiative efficiency increase markedly, so that a larger fraction of the available power can be extracted. Enhancement of the $O_2(a)$ yield will also increase the laser power and efficiency by allowing more recycling of the I atoms within the optical resonator.

5. KINETICS MODELING AND DISCUSSION

We have assembled a kinetics model using the FLUENT CFD calculations to define the pressures, temperatures, and flow velocities in the subsonic and supersonic flow fields. For simplicity, we have used the on-axis values for these quantities. Although the FLUENT flowfield calculations are for non-reacting flow, we expect them to be reasonably representative for reacting flow owing to the high dilution with helium.

As an initial elementary reaction set, we have used the conventional EOIL mechanism as shown in Table 1, including dissociation of I_2 and IO by O, reversible energy transfer between $O_2(a)$ and I to excite I*, quenching of I* by O, and removal of O by reactions with NO and NO_2. Rate coefficients for these key reactions are all well known, at least near room temperature.[11] We have also included several minor reactions to account for quenching of I* by NO, I_2, and $O_2(a)$, and energy transfer among $O_2(a)$, $O_2(b)$ and I_2, however these reactions have little significance for our range of experimental conditions. Rather than add the complexity of modeling the discharge production of $O_2(a)$ and O, we have omitted the discharge chemistry and specified initial $O_2(a)$ and O yields consistent with our data. We have also omitted the chemistry of enhancement of $O_2(a)$ by NO reactions, since this would be highly speculative[10] and appears to be a small effect in our experiments. We have focused on the low flow rate condition, 45 mmole/s with 5% O_2/He, initial $O_2(a)$ and O yields of 20%, and $[I_2]_o$ values from 2×10^{13} cm^{-3} to 3×10^{15} cm^{-3}, with injection of the I_2 (instantaneously mixed) 8 cm upstream of the nozzle throat (~1 ms reaction time) as in the experiments. The initial NO concentration was optimized for maximum gain at each $[I_2]_o$. We did not include any mixing or diffusion effects.

Examples of predicted subsonic and supersonic gain profiles for low $[I_2]_o$ are shown in Figure 12, illustrating the kinetics effects of atomic oxygen and the addition of NO. The presence of atomic oxygen substantially reduces the gain from the unquenched value. However, even for an O yield as high as 30%, the predicted supersonic gain is still positive, in clear contrast with our data. Addition of NO brings the gain almost up to the unquenched level, regardless of the

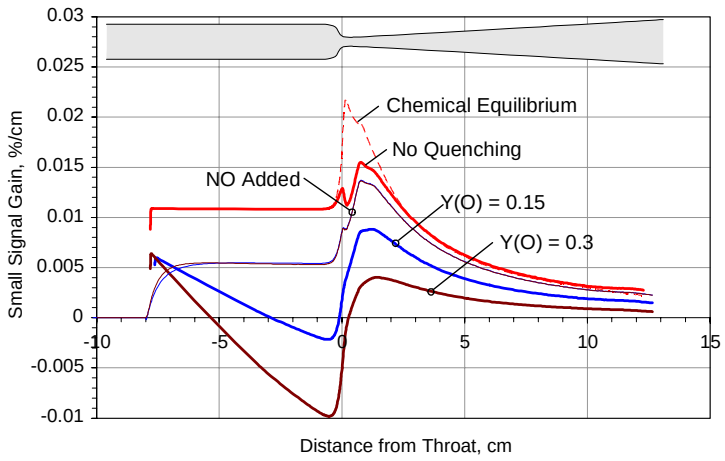

Figure 12. Predicted subsonic and supersonic gain profiles for the Reaction set of Table 1.

initial O yield. Also shown in Figure 12 is the effect of finite chemical relaxation in our flow. The uppermost gain profile is based on the [I*]/[I] ratio determined by chemical equilibrium with the numerically computed $[O_2(a)]/[O_2]$ ratios and temperatures in the flow for the unquenched case. The contrast between the "equilibrium" and "unquenched" cases illustrates the flow distance required for the reaction rates to fully adjust to the rapidly decreasing temperature and pressure in the supersonic flow. This is primarily due to the greatly reduced rate coefficient for Reaction (-1) at lower temperatures. Calculated dependences of gain and O-yield on NO are shown in Figure 13, for comparison to the experimental results in Figure 8. The predicted gain at optimum NO is roughly comparable to the observed values. However, at higher $[I_2]_o$, the computed gains are larger than the observed values. In addition, the calculated profiles have a pronounced peak ~1 cm downstream of the throat, while the observed profiles tend to be much flatter and peaked toward 4 cm. Predicted scaling of gain with $[I_2]_o$ is shown in Figure 14, for our low-flow-rate experimental conditions and injection of I_2 8 cm upstream of the throat. The reaction set of Table 1 predicts small but positive gain at low $[I_2]_o$ without NO, and considerable enhancement of the gain by addition of optimum NO. The roll-off at high $[I_2]_o$ results from failure of the I_2 dissociation process due to over-titration of O by I_2. (For our current discharge yields, there is not enough $O_2(a)$ in the flow to effectively dissociate the I_2.) The computed gains are clearly limited by the partially arrested O + I* quenching throughout. Reduction of the subsonic reaction distance should allow scaling to higher gains, provided there is adequate mixing and I_2 dissociation.

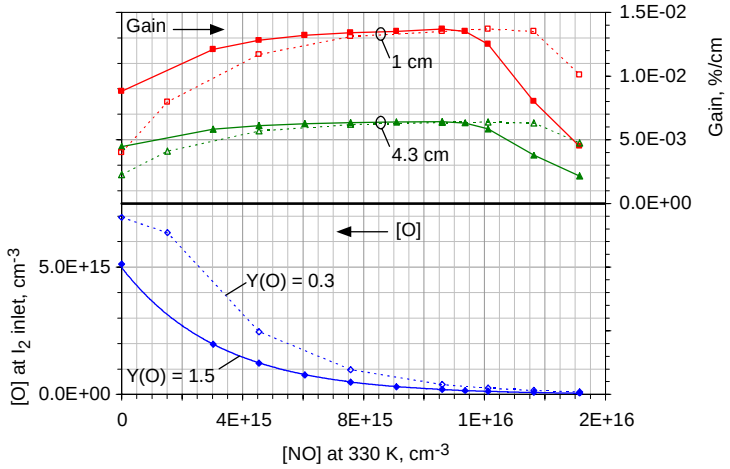

Figure 13. Predicted dependence of gain and O yield on NO, for O yield = 15% (solid lines) and 30% (dashed lines). Gain predictions are shown for 1 cm and 4.3 cm downstream of the nozzle throat.

The observation of net absorption at low $[I_2]_o$ without NO, where O + I* quenching is clearly negligible, suggests strongly that there is an additional, unknown loss process for I*. We previously noted a similar effect in subsonic discharge-flow reactor experiments at 1-3 torr.[5,7] In addition, in the present MIDJet experiments, we have observed that the $O_2(a)$ loss in the mixing region is entirely consistent with the O + I* mechanism alone, and is ameliorated by the addition of NO as expected. This indicates that the additional loss of I* somehow occurs without concomitant loss of $O_2(a)$. This implies production of $O_2(a)$, i.e. the loss mechanism may have the net form I* + X → I + $O_2(a)$ + Y. The identities of X and Y are open to speculation, however X must be present in fairly large concentration and must have a large rate coefficient for I* quenching. Our preliminary estimate of this first-order loss rate for the 45 mmole/s condition is ~1.5 x 10^5 s^{-1}. As another alternative, perhaps the observations could be accounted for by a substantially larger rate coefficient for the O + I* quenching reaction at low temperatures. More detailed modeling calculations are in progress.

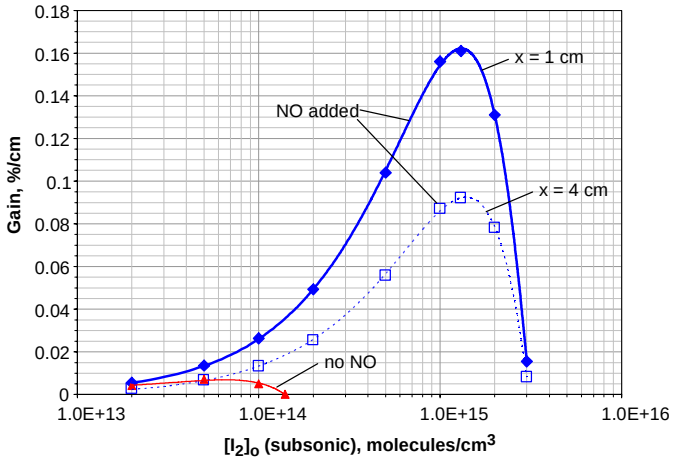

Figure 14. Predicted scaling of gain with initial I_2 concentration in the subsonic flow, for the present reactor configuration: I_2 injection 8 cm upstream of the nozzle throat (1 ms reaction time), flow conditions as described in the text.

6. SUMMARY

We have described a supersonic, microwave-discharge, oxygen-iodine laser reactor, and initial observations of gain and lasing for 1 kW discharge power. We have observed lasing for total flow rates up to 82 mmole/s and discharge pressures up to 70 torr. The principle observations are:

The commonly accepted EOIL reaction set, incorporating quenching of I* by O, does not fully account for observed I* loss in the reaction of active-O_2 with I_2. We estimate the additional first-order loss rate of I* is on the order of 10^5 s^{-1}. Addition of NO appears to ameliorate this loss at least partially, but perhaps not completely.

Addition of NO is required to achieve optical gain and lasing in our present configuration. We have identified the effects of NO on the balancing of O concentrations between I* quenching and I_2 dissociation. The observed gain is strongly dependent on the NO flow rate. The optimum NO flow rate decreases with increasing I_2 flow rate.

The O concentration must be maintained in excess of the initial I_2 concentration to ensure adequate I_2 dissociation in the subsonic reaction zone. However, the $O_2(a)$ loss rate due to O + I* quenching scales as [O][I], and thus becomes a more severe limitation at higher I_2. Use of shorter subsonic reaction distances and pre-dissociation of I_2 by a secondary discharge would likely relieve much of this kinetic limitation on the gain scaling.

Optical gains of at least ~0.2 %/cm will enable large increases in power extraction efficiency. The kinetics of the stimulated emission within the resonator volume are an important consideration.

ACKNOWLEDGEMENTS

This research is supported by the Air Force Research Laboratory under Contract FA9451-06-C-0196. We are grateful for many excellent technical discussions with Tim Madden and David Hostutler of AFRL, David Carroll and Joe Verdeyen of CU Aerospace, Wayne Solomon of UIUC, Michael Heaven of Emory University, Glenn Perram of AFIT, and George Caledonia, B. David Green, Larry Piper, Hart Legner, and Mike Read of PSI.

REFERENCES

[1] Carroll, D. L., Verdeyen, J. T., King, D. M., Zimmerman, J. W., Laystrom, J. K., Woodard, B. S., Benavides, G. F., Kittell, K., and Solomon, W. C., "Path to the Measurement of Positive Gain on the 1315-nm Transition of Atomic Iodine Pumped by $O_2(a^1\Delta)$ Produced in an Electric Discharge," IEEE J. Quantum Electron. 41, 213-223 (2005).

[2] Carroll, D. L., Verdeyen, J. T., King, D. M., Zimmerman, J. W., Laystrom, J. K., Woodard, B. S., Benavides, G. F., Richardson, N. R., Kittell, K., and Solomon, W. C., "Studies of CW Laser Oscillation on the 1315-nm Transition of Atomic Iodine Pumped by $O_2(a^1\Delta)$ Produced in and Electric Discharge," IEEE J. Quantum Electron. 41, 1309-1318 (2005).

[3] Benavides, G. F., Palla, A. D., King, D. M., Carroll, D. L., Verdeyen, J. T., Laystrom, J. K., Field, T. H., Zimmerman, J. W., Woodard, B. S., and Solomon, W. C., "Hybrid ElectricOIL Discharge, Gain, and Power Enhancements," AIAA 2007-4623, 38th AIAA Plasmadynamics and Lasers Conference, Miami, FL, June 2007.

[4] Rawlins, W. T., Lee, S., Kessler, W. J., and Davis, S. J., "Observations of Gain on the I($^2P_{1/2}\rightarrow{}^2P_{3/2}$) Transition by Energy Transfer from $O_2(a^1\Delta_g)$ Generated by a Microwave Discharge in a Subsonic Flow Reactor," Appl. Phys. Lett. 86, 051105 (2005).

[5] Rawlins, W. T., Lee, S., Kessler, W. J., Piper, L. G., and Davis, S. J., "Advanced Diagnostics and Kinetics of Oxygen-Iodine Laser Systems," AIAA-2005-5299, 36th AIAA Plasmadynamics and Lasers Conference, Toronto, Ontario, Canada, June 2005.

[6] Rawlins, W. T., Lee, S., Kessler, W. J., Oakes, D. B., Piper, L. G., and Davis, S. J., "The Electric Oxygen-Iodine Laser: Chemical Kinetics of $O_2(a^1\Delta)$ Production and I($^2P_{1/2}$) Excitation in Microwave Discharge Systems," Proc. SPIE Paper 6101C-51, LASE 2006 High-Energy/Average Power Lasers and Intense Beam Applications, San Jose CA, January 2006.

[7] Rawlins, W. T., Lee, S., and Davis, S. J., "Kinetics of Oxygen Discharges and I($^2P_{1/2}$) Excitation for EOIL," Proc. SPIE Paper 6454-18, LASE 2007 High-Energy/Average Power Lasers and Intense Beam Applications, San Jose CA, January 2007.

[8] Rawlins, W. T., Caledonia, G. E., and Armstrong, R. A., "Dynamics of Vibrationally Excited Ozone Formed by Three-Body Recombination. II. Kinetics and Mechanism," J. Chem. Phys. 87, 5209-5221 (1987).

[9] Zimmerman, J. W., King, D. M., Palla, A. D., Verdeyen, J. T., Carroll, D. L., Laystrom, J. K., Benavides, G. F., Woodard, B. S., Solomon, W. C., Rawlins, W. T., Davis, S. J., and Heaven, M. C., "Important Kinetic Effects in the Hybrid ElectricOIL System," SPIE Vol. 6261, 62611R (2006).

[10] Rawlins, W. T., Lee, S., and Davis, S. J., "Production of Metastable Singlet Oxygen in the Reaction of Nitric Oxide with Active Oxygen," Proc. SPIE Paper 6874-8, LASE 2008 High Energy/Average Power Lasers and Intense Beam Applications III, San Jose, CA, January 2008.

[11] Palla, A. D., Zimmerman, J. W., Woodard, B. S., Carroll, D. L., Verdeyen, J. T., Lim, T. C., Rawlins, W. T., Lee, S., Davis, S. J., and Solomon, W. C., "Oxygen Discharge and Post-Discharge Kinetics Experiments and Modeling for the ElectricOIL System," Proc. SPIE Vol. 6454, Paper 19, LASE 2007 High-Energy/Average Power Lasers and Intense Beam Applications, San Jose CA, January 2007.